*Inorg. Chem.* **2006**, *45*, 3837–3839


# Polymorphic Alternating HNN–Cobalt(II) Chains Both Behaving as Single-Chain Magnets (HNN = 4,4,5,5-Tetramethylimidazolin-1-oxyl 3-Oxide)

**Norio Ishii,[†] Takayuki Ishida,*[,†,‡] and Takashi Nogami[†]**

*Department of Applied Physics and Chemistry and Course of Coherent Optical Science, The University of Electro-Communications, Chofu, Tokyo 182-8585, Japan*

Received December 12, 2005

Metal-radical alternating chains $[Co(hfac)_2HNN]_n$ crystallized in two morphs containing repeating all-cis ($\alpha$) and cis,cis,trans ($\beta$) configurations with respect to the $O_{HNN}$–Co–$O_{HNN}$ geometry (HNN = 4,4,5,5-tetramethylimidazolin-1-oxyl 3-oxide). Both phases showed magnetization jumps with hysteresis at 2 K. The $\alpha$ phase has a relatively high activation energy of magnetization reorientation (193 K).

There have been ample examples of alternating one-dimensional (1D) complexes containing nitronyl and imino nitroxide radicals (Chart 1a) with metal hfac salts[1] in pursuit of metal-radical hybrid magnets (hfac stands for 1,1,1,5,5,5-hexafluoropentane-2,4-dionate). We assume that the choice of small ligands and anions is crucial in order to bestow strong exchange interaction, and accordingly high $T_c$, on bulk magnetic materials. Actually, we have developed the minimal bridges HNN and HIN for strongly coupled systems, $[Mn^{II}(hfac)_2L]_n$ (L = HNN, HIN).[2] On the other hand, Gatteschi et al. reported the single-chain magnets (SCMs) using somewhat bulky NN bridges such as $[Co^{II}(hfac)_2$(*p*-methoxyphenyl-NN)$]_n$ (**1**)[3] and $[Dy^{III}(hfac)_3$(*p*-phenoxyphenyl-NN)$]_n$.[4] Slow magnetic relaxation in SCMs requires the condition that the ratio of the intrachain interaction over the interchain interaction must be high.[3] The short HNN bridge might satisfy the requirement of larger intrachain interactions, whereas bulky RNN bridges were supposed to be suitable for smaller interchain interactions. To clarify whether the former requirement outweighs the latter, we investigated the magnetic properties of $[Co^{II}(hfac)_2HNN]_n$ (**2**). A few examples of $Co^{II}$-based SCMs are known so far.[3,5]

**Chart 1.** Structural Formulas

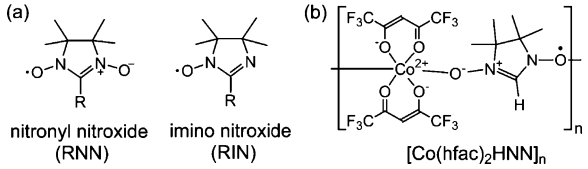


Complexation of $Co(hfac)_2$ with HNN[6] was conducted according to the method reported for the $Mn^{II}$ analogue,[2] giving two phases of **2**. Platelet crystals ($\alpha$ phase) were preferentially obtained from heptane−ether, while needlelike crystals ($\beta$ phase) were obtained from ether−dichloromethane, but they did not contain solvate molecules.[7] Each phase was separately prepared, and the crystal structure and magnetic properties were investigated.

Figure 1a shows a chain structure of $\alpha$-**2** determined in a monoclinic $P2_1/c$ space group. A pair of HNN and $Co(hfac)_2$ is a crystallographically independent unit. Each Co ion is hexacoordinated by four O atoms of two hfac moieties and by two O atoms of two different HNN radicals. The bond lengths of Co−$O_{HNN}$ are 2.084(3) and 2.083(3) Å. Two HNN O atoms are coordinated in a cis configuration with an $O_{HNN}$−Co−$O_{HNN}$ angle of 88.4(1)°. The chain runs along the crystallographic *b* axis.

Another phase $\beta$-**2** has a monoclinic $C2/c$ space group. The crystallographically independent unit corresponds to one and a half formula units (Figure 1b). An inversion center resides at Co2, and accordingly two HNN O atoms are coordinated to Co2 in a trans manner, giving a cis,cis,trans configuration as a repeating unit. The cis $O_{HNN}$−Co−$O_{HNN}$ angle is 90.7(1)°. The $O_{HNN}$−Co bond lengths are 2.059(4)−2.083(4) Å. The chains are located parallel to the crystallographic $a-c$ diagonal direction.

* To whom correspondence should be addressed. E-mail: ishi@pc.uec.ac.jp.
[†] Department of Applied Physics and Chemistry.
[‡] Course of Coherent Optical Science.

(1) Caneschi, A.; Gatteschi, D.; Sessoli, R. *Acc. Chem. Res.* **1989**, *22*, 392. Caneschi, A.; Gatteschi, D.; Rey, P. *Prog. Inorg. Chem.* **1991**, *39*, 33.
(2) Ise, T.; Ishida, T.; Hashizume, D.; Iwasaki, F.; Nogami, T. *Inorg. Chem.* **2003**, *42*, 6106.
(3) Caneschi, A.; Gatteschi, D.; Lalioti, N.; Sangregorio, C.; Sessoli, R.; Venturi, G.; Vindigni, A.; Rettori, A.; Pini, M. G.; Novak, M. A. *Angew. Chem., Int. Ed.* **2001**, *40*, 1760.
(4) Bogani, L.; Sangregorio, C.; Sessoli, R.; Gatteschi, D. *Angew. Chem., Int. Ed.* **2005**, *44*, 5817.
(5) Liu, T.-F.; Fu, D.; Gao, S.; Zhang, Y.-Z.; Sun, H.-L.; Su, G.; Liu, Y.-J. *J. Am. Chem. Soc.* **2003**, *125*, 13976. Pardo, E.; Ruiz-García, R.; Lloret, F.; Faus, J.; Julve, M.; Journaux, Y.; Delgado, F.; Ruiz-Pérez, C. *Adv. Mater.* **2004**, *16*, 1597.
(6) Ullman, E. F.; Call, L.; Osiecki, J. H. *J. Org. Chem.* **1970**, *35*, 3623.
(7) The two polymorphic phases could not be converted to each other.

10.1021/ic052119k CCC: $33.50 
Published on Web 04/18/2006

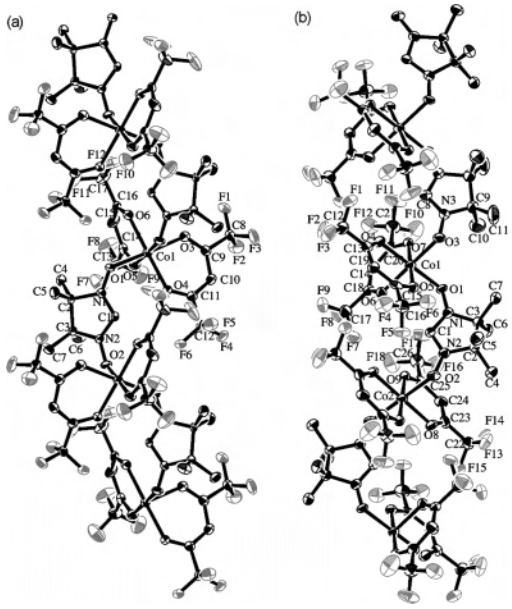

**Figure 1.** ORTEP drawings of four repeating units in the infinite chains of (a) α-**2** and (b) *β*-**2**. The thermal ellipsoids are drawn at the 50% probability level. H atoms are omitted.

The intrachain Co−Co distances are 6.8677(8) Å for α-**2** and 6.4408(8) and 6.616(1) Å for *β*-**2**, which are much shorter than that of **1** (7.82 Å).[3] Owing mainly to different M−O bond lengths, they are slightly shorter than the intrachain Mn−Mn distances (7.08 and 7.19 Å) in [Mn(hfac)$_2$(HNN)]$_n$ (**3**).[2] The shortest interchain Co−Co distances are 9.0448(9) and 9.428(1) Å for α- and *β*-**2**, respectively, which are also much shorter than that of **1** (11.29 Å).[3] Complex **3** has a different packing motif, and the corresponding distance is reported to be 8.35 Å.[2]

Magnetic properties of randomly oriented polycrystalline samples were measured on a SQUID magnetometer. The temperature dependence of $\chi_m T$ measured at 500 Oe for both phases showed upsurge on cooling like the Mn analogue.[2] The magnetization saturation values are ca. $1.3 \times 10^4$ erg Oe$^{-1}$ mol$^{-1}$ at 2 K for both phases, which corresponds to $S_{total} = 1$ with $g_{ave} = 2.3$ for the formula unit. These findings indicate that the chains are ferrimagnetic. Because the octahedral Co$^{II}$ ion has a d electron configuration of $(t_{2g})^5(e_g)^2$, orbital overlaps between the magnetic orbitals of Co d$\pi(t_{2g})$ and HNN $\pi^*$ should be appreciable, giving rise to antiferromagnetic coupling. The plots of $\chi_m T$ vs $T$ and anisotropic magnetization ($M_{||chain}$ and $M_{\perp chain}$) vs $T$ for each phase are given in Figures 1S and 2S in the Supporting Information, respectively.

Single-crystal magnetic studies for both phases exhibited a remarkable Ising-type anisotropy in the chain direction. Hereafter magnetic properties were measured on a single crystal or aligned single crystals with a magnetic field applied parallel to the chain direction.

Figure 2a shows the results of FCM (field-cooled magnetization), RM (remnant magnetization), and ZFCM (zero-field-cooled magnetization) on α-**2**. The ZFCM curve approached the FCM one, and the RM decreased on heating. Note that these profiles depended on the temperature scan rate. The results on *β*-**2** (Figure 2b) showed the complete

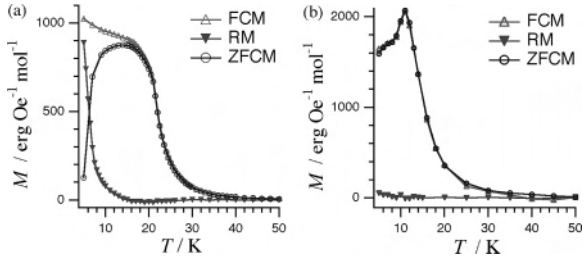


**Figure 2.** FCM, RM, and ZFCM for (a) α- and (b) *β*-**2** in a temperature range of 5−50 K. A single crystal was used in each experiment. Applied fields were 5 and 30 Oe for α- and *β*-**2**, respectively.

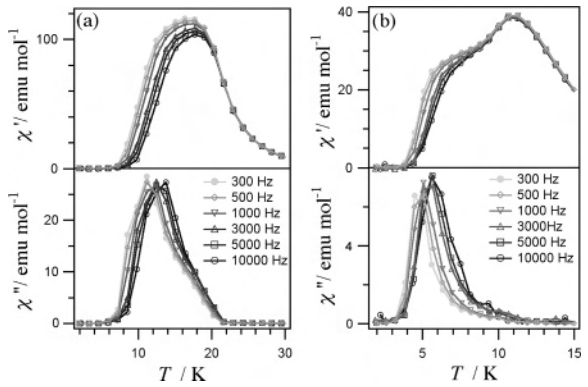


**Figure 3.** Frequency dependence of $\chi_{ac}'$ (top) and $\chi_{ac}''$ (bottom) for (a) α- and (b) *β*-**2** measured on a single crystal.

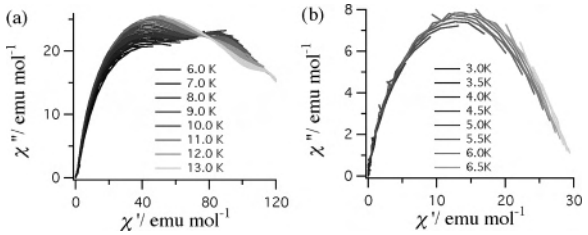


**Figure 4.** Cole−Cole diagrams for (a) α- and (b) *β*-**2**.

absence of RM and coincidence between ZFCM and FCM, indicating a much faster relaxation than that of α-**2** and also than the time scale of the measurements (several minutes for each data point). Actually, we could observe the remnance of *β*-**2** below 3 K as shown below.

To clarify the relaxation behavior, we measured the frequency dependence of $\chi_{ac}'$ and $\chi_{ac}''$, which represent in-phase and out-of-phase parts, respectively, of ac magnetic susceptibility. Figure 3a shows the results on α-**2**. An increase of $\chi_{ac}''$ was found together with a concomitant decrease of $\chi_{ac}'$ on cooling below 22 K, indicating a slow relaxation of the magnetization. $\chi_{ac}''$ exhibited a peak at around 13 K, and the peaking temperature was elevated with an increase of the frequency. According to the Cole−Cole analysis,[8] two humps are found in the plot of $\chi_{ac}''$ vs $\chi_{ac}'$ for α-**2** (Figure 4a).

The $\chi_{ac}'$ curve of *β*-**2** showed a frequency-independent peak at 11 K and a frequency-dependent shoulder around 6 K (Figure 3b). The $\chi_{ac}''$ behaved similar to that of α-**2**, but the peak occurred at a lower temperature. In contrast to the case of α-**2**, a semicircle is clearly drawn in the Cole−Cole

(8) Cole, K. S.; Cole, H. R. *J. Chem. Phys.* **1941**, *9*, 341.

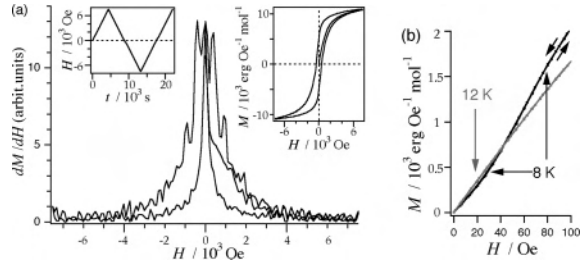


**Figure 5.** (a) Differential magnetization curve for a single crystal of α-**2** measured at 4.43 K with a constant field-sweeping rate of $1.7 \times 10^{-4}$ T $s^{-1}$. Left inset: field-sweeping sequence. Right inset: hysteresis curve. (b) Magnetization curves of $\beta$-**2** measured at 8 and 12 K. Several aligned single crystals were used with a field-sweeping rate of $9.6 \times 10^{-6}$ T $s^{-1}$.

plot for $\beta$-**2** (Figure 4b), suggesting that the $\chi_{ac}'$ decrease and $\chi_{ac}''$ increase are due to a single relaxation process.

The relaxation rate ($1/\tau$) is equal to the frequency of the applied ac field ($2\pi\nu$) at the temperature of the maximum of $\chi_{ac}''$. The temperature dependence of $\tau$ can be obtained from each $\chi_{ac}''$ curve (Figure 3 (bottom)). The energy barrier ($\Delta$) of the magnetization reorientation could be analyzed based on an Arrhenius-type equation,[9] $\ln(2\pi\nu) = -\ln(\tau_0) - \Delta/k_BT$, giving $\Delta/k_B = 193$ K and $\tau_0 = 1.3 \times 10^{-12}$ s for α-**2** and $\Delta/k_B = 71$ K and $\tau_0 = 1.1 \times 10^{-10}$ s for $\beta$-**2**. The $\Delta$ value of α-**2** was higher than that of **1**.[3]

We measured the RM decay as a function of time (Figure 3S in the Supporting Information). The observed magnetization was expressed as $M_{obs} = M_{SCM} \exp[-(kt)^{\gamma}]$, where the parameter $\gamma$ has been introduced as a coefficient for the stretched exponential.[10,11] According to this analysis, the relaxation rate constant $k$ of α-**2** was determined and the Arrhenius plot gave the activation energy, $\Delta'/k_B$, calculated to be 162 K with $\tau_0 = 4.8 \times 10^{-9}$ s. This value does not agree with that of the ac magnetic susceptibility measurements. The reason simply lies in the presence of two relaxation processes, as indicated by the Cole−Cole plot (Figure 4a); one is operative in the temperature range for the ac measurements (10−15 K) and the other in that for the dc measurements (4−10 K).

Similar analysis from the RM decay on $\beta$-**2** in a temperature range of 1.8−2.9 K revealed the activation energy to be 61 K ($\tau_0 = 9.3 \times 10^{-9}$ s). This value seems consistent with that of the ac measurements described above within a possible error due to the narrow temperature range of this experiment.

The magnetization jumps were observed in hysteresis curves, being usually related with quantum tunneling of magnetization.[3,5,9] Figure 5a shows that the jumps took place at $H = 0$, 0.04, and 0.09 T for α-**2** measured at 4.43 K. Detailed differential magnetization plots (Figure 4S in the Supporting Information) revealed the jumps at 0, 1.1, and 1.8 T for α-**2** and 0 and 0.4 T for $\beta$-**2** at 2.0 K. The position of the steps hardly depended on the temperature between 2.0 and 3.0 K for the former. We measured the hysteresis curves at 2.0 K with the field-sweeping rates of $7.4 \times 10^{-4}$ and $1.3 \times 10^{-3}$ T $s^{-1}$ for the latter and found a very slight shift of the step position. The apparent coercive field ($H_c$) of α-**2** at 2 K was 2.0 T, which is much larger than that of **1** (ca. 1 T).[3] On the other hand, $\beta$-**2** exhibited a narrower hysteresis with $H_c$ of 0.25 T at 2 K. This finding implies that α- and $\beta$-**2** had slower and faster relaxations, respectively, than that of **1**, being consistent with the estimation of $\Delta$, though the shape of the hysteresis depends also on the tunneling probability.

Interestingly, we observed the cusp at 11 K in the $\chi_{ac}'$ plot of $\beta$-**2** (Figure 3b (top)) and also in the dc FCM measurement (Figure 2b). We measured magnetization curves with temperature varied around 11 K. An S-shaped curve was clearly drawn in both directions of applying and removing a magnetic field at 8 K, whereas a linear feature was observed at 12 K (Figure 5b). This finding suggests the presence of a critical point at 11 K for $\beta$-**2**. We suppose a possibility that a metamagnetic-like transition would take place because interchain antiferromagnetic coupling is as small as ca. 0.005 T. However, we could not characterize a ground Néel state below 11 K in the ac/dc magnetic measurements, and no anomaly was found in heat capacity measurements of $\beta$-**2**. Although a possible phase transition could not be eliminated completely, it is most likely that this behavior would originate in the finite-size effects[12] of the 1D Ising system in a paramagnetic phase.[13] The double-peak feature in the $\chi_{ac}'$ vs $T$ plot can be described as superposed magnetic properties due to an infinite SCM and precursory fragmental chains.

The absence of such an anomaly for α-**2** might be due to the structural uniformity in the all-cis chain, whereas the cis,-cis,trans mixed configuration of $\beta$-**2** favors a shorter size of fragmental chains. Further, this structural feature seems responsible for the characteristics of SCMs; α-**2** has the higher $\Delta$ and longer $\tau$ than $\beta$-**2**.

Metal-radical hybrid magnets such as **3** have often been exploited in pseudo-1D systems.[2] On the other hand, the magnetically discrete 1D structures of **2** behaved as SCMs. In conclusion, the minimal bridging ligand, HNN, is a versatile building block for the development of both bulk magnets and SCMs.

**Acknowledgment.** This work was supported by Grants-in-Aid for Scientific Research (Grants 15073101, 16550121, and 15550115) from the Ministry of Education, Culture, Sports, Science and Technology, Japan.

**Supporting Information Available:** CIF files for α- and $\beta$-**2**, including the experimental conditions on the X-ray diffraction and tables of selected distances and angles, and Figures 1S−4S for detailed magnetic measurements. This material is available free of charge via the Internet at http://pubs.acs.org.

IC052119K

(9) Clérac, R.; Miyasaka, H.; Yamashita, M.; Coulon, C. *J. Am. Chem. Soc.* **2002**, *124*, 12837.
(10) Thomas, L.; Caneschi, A.; Barbara, B. *Phys. Rev. Lett.* **1999**, *83*, 2398.
(11) Gatteschi, D.; Sessoli, R. *Angew. Chem., Int. Ed.* **2003**, *42*, 268.
(12) Bogani, L.; Sessoli, R.; Pini, M. G.; Rettori, A.; Novak, M. A.; Rosa, P.; Massi, M.; Fedi, M. E.; Giuntini, L.; Caneschi, A.; Gatteschi, D. *Phys. Rev. B* **2005**, *72*, 064406.
(13) Caneschi, A.; Gatteschi, D.; Lalioti, N.; Sangregorio, C.; Sessoli, R.; Venturi, G.; Vindigni, A.; Rettori, A.; Pini, M. G.; Novak, M. A. *Europhys. Lett.* **2002**, *58*, 771.